Classification of crystal defects in multicrystalline silicon solar cells and wafer using spectrally and spatially resolved photoluminescence

D. Lausch,[1,a] T. Mehl,[2] K. Petter,[3] A. Svarstad Fløa,[2] I. Burud,[2] and E. Olsen[2]
[1]*Fraunhofer-Center für Silizium Photovoltaik CSP, Otto-Eißfeldt-Straße 12, 06120 Halle (Saale), Germany*
[2]*Norwegian University of Life Sciences NMBU, Universitetstunet 3, 1430 Ås, Norway*
[3]*Hanwha Q CELLS GmbH, OT Thalheim, Sonnenallee 17–21, 06766 Bitterfeld-Wolfen, Germany*

(Received 30 October 2015; accepted 12 January 2016; published online 3 February 2016)

In this contribution, spectral photoluminescence (SPL) imaging detecting both the spectral distribution and the lateral position is applied on recombination active defects in multicrystalline silicon solar cells and wafers. The result is analysed by a Multivariate Curve Resolution (MCR) algorithm using the spectral photoluminescence response and their positions. (i) Without any pre-assumptions made, the algorithm distinguishes four different recombination active defect types. Looking at the spatial distribution, it is shown that two of these defect types coincide with two defect types that have been distinguished on solar cell level using an analysis of forward and reverse biased electroluminescence (denoted as Type-A and -B) previously. (ii) Using SPL, all previously classified defects can also be distinguished at the wafer level. Therefore, the defects limiting the solar cell efficiency are already present in the wafer material and not introduced by the solar cell process. This is of particular interest for the question of how to predict the solar cell efficiency based on the PL measurements at the wafer level. The SPL is able to distinguish between the recombination activity of the dominant Type-A and -B defects that cannot be distinguished by classical PL measurements of the band-to-band recombination at the wafer level. The technique also highlights the changes in recombination activity of the given defects throughout the fabrication process. (iii) Additionally, it is shown that the spectral peak positions of Type-A defects coincide with the known D3 and D4 lines and of Type-B defects with the D1 line on both solar cell and wafer level. Two further defects are captured by the MCR algorithm denoted as Type-VID3 and Type-D07 defects occurring as spot-like defects in isolated positions. Their spectral PL response is analysed as well. © *2016 AIP Publishing LLC*. [http://dx.doi.org/10.1063/1.4940711]

I. INTRODUCTION

Currently, more than 60% of all solar modules are made from wafer-based multicrystalline silicon (mc-Si) solar cells. However, the efficiency of mc-Si solar cells is ∼10%–15% lower compared to that of the monocrystalline Si solar cells. A major reason for this is the presence of different recombination-active crystal defects in mc-Si materials. These defects have a negative influence on the efficiency[1–3] and electrical breakdown behavior of the cells.[4–6] To overcome these disadvantages, the physical mechanisms taking place at these defect sites must be understood systematically. Single defects in silicon solar cells have been investigated for several years.[7–12] Recently, a systematic investigation for different types of efficiency limiting crystal defects from 6″ solar cells down to the atomic level has been performed based on a classification scheme related to electroluminescence and pre-breakdown behaviour of crystal defects.[13] The recombination active defects were locally distinguished into Type-A and Type-B defects. Type-A defects were correlated to metal (iron) impurities activated by temperature treatment[14] with high impact on the solar cell efficiency.[15] On the contrary, Type-B defects show only a low influence on the efficiency. The root cause of Type-B defects is still unclear. Recombination models for both defect types were proposed.

Photoluminescence (PL) imaging is an established method for characterization of mc-Si wafers by locating recombination active defects at the solar cell[16] and wafer level.[17] Typically, it is performed by integrating all photon energies higher than the smallest energy (longest wavelength) detectable by the camera used. Defected regions are characterized by different luminescence intensities. However, to understand the physical mechanisms occurring at the localized defects the spectral luminescence distributions are needed. For this, a spectral PL imaging technology (SPL) has been developed where both the spectral distribution and lateral information are recorded in a so-called hyperspectral cube containing an image of the sample at each resolved wavelength.[18] In order to analyse the spatial and spectral data, Multivariate Curve Resolution (MCR) was applied in order to extract all the emission signals simultaneously across the wafer, as demonstrated in Ref. 19.

In this work, we apply the spectral imaging method to 6″ mc-Si silicon solar cells and neighbouring wafers. The result is analysed by the MCR method. In Section III A, it is shown that the recombination active defects of the solar cells are distinguished by the MCR algorithm into four different defect types. Two of the types were found to be present at the same positions like type A and B defects as introduced in

[a]Author to whom correspondence should be addressed. Electronic mail: dominik.lausch@csp.fraunhofer.de

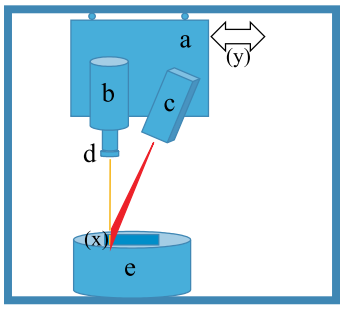

FIG. 1. Schematic illustration of the SPL method. A computer controlled translational stage (a) is used to move the hyperspectral camera (b) relative to the sample (y-direction). The sample is located on an aluminium surface on top of a cryogenic cooler (e). A line laser (c) excite electrons on the line (x-direction) sensed by the camera. A long pass filter (d) is used to stop the exciting signal to enter the camera.

Ref. 13 by forward and reverse biased electroluminescence. The SPL procedure is then applied to a neighbouring as-cut mc-Si wafer in Sec. III B. It is known that the same classified defects are already present in the wafer material, so that type A and B defect regions can already be distinguished on the wafer level. Therefore, the root cause of these defects is the Si bulk material rather than the solar cell process. In Section III C, the spectral response of each defect type is shown. The paper is concluded by a discussion in Section IV. All investigations were performed on standard 6″ solar cell or wafer size. Investigations with high lateral magnification will be focused on an upcoming publication.

II. EXPERIMENTAL DETAILS

Samples: The mc-Si solar cells were fabricated in 2009 with a standard commercial process at the company Q-Cells SE based on Boron-doped (acceptor concentration $N_A \sim 10^{16}\,cm^{-3}$) 156 mm × 156 mm mc-Si wafers made from standard electronic grade silicon with comparable high purity. The wafers analysed were neighbouring unprocessed wafers of the same type hence exactly out of the same crystal region of the ingot.

Spectral imaging (SPL): SPL images of the samples were obtained using a near-infrared (NIR) hyperspectral camera (SWIR, Specim, Finland). The setup is depicted in Figure 1. A mercury cadmium telluride detector is used with spectral sensitivity in the 929–2531 nm (0.49–1.33 eV) range with a resolution of 6 nm (256 bands). A line image is recorded (320 pixels) giving a spatial resolution of 0.5 mm in both the x and y directions in the setup for this study. 3D images with one spectral and two spatial dimensions were obtained by scanning the imaged line across the samples. As an excitation source, an 808 nm line laser was used with an irradiated power density of 2 W/cm^2 (Lasiris Magnum II). An 850 nm low-pass filter prevented laser beam reflections from entering the optic apparatus. The samples were cooled to 90 K on a polished aluminium surface on top of a cryogenic cooler filled with liquid nitrogen in order to be able to separate single defect lines with high energetic resolution. With increasing temperature, the spectral response of a defect level is energetically broadened resulting in a strong overlap of the different spectral responses. At room temperature, only a broad defect luminescence within the band gap can be detected. Similar setups have been used in previous studies.[19–22]

Data processing: MCR is a mathematical method for deconvolving complex, convoluted signals being composed of several discrete, simultaneously occurring signals. The method involves decomposing the recorded data (signal) matrix D into a matrix containing all the individual signals S^T and a weight matrix C where each signal from S^T is weighted to form the recorded signal in D. Residuals are contained in a separate matrix E. The mathematical representation of the method can be described by the following equation:

$$D = CS^T + E.$$

Initially, the number of components in C and S^T is estimated and put into the model. An iterative process then optimizes the matrixes to best fit D while minimizing the content in E by an Alternating Least Squares (ALS) algorithm.[23]

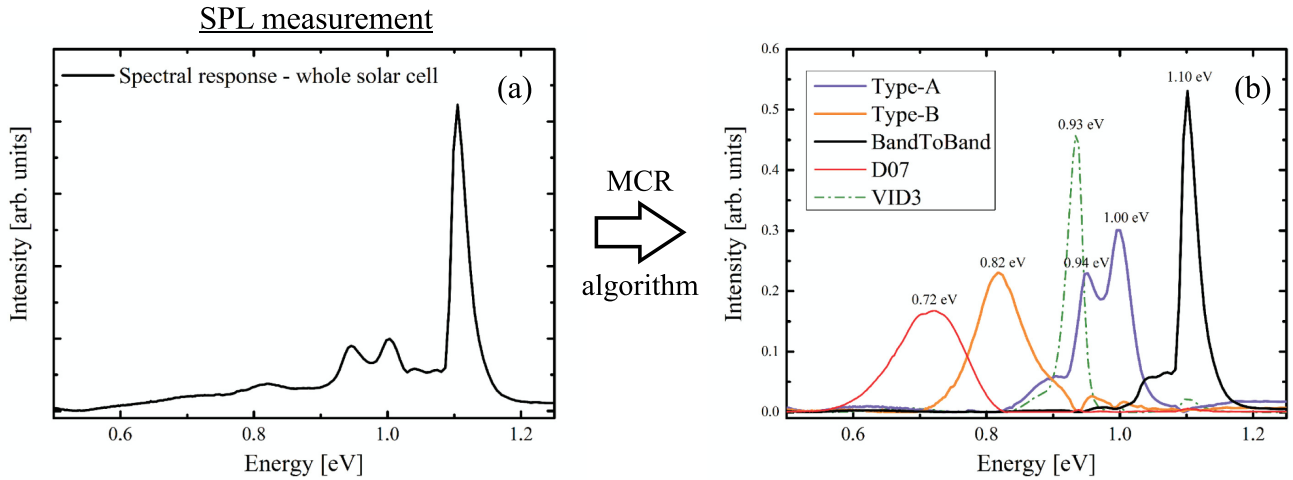

FIG. 2. (a) Spectral response of a solar cell integrated over the whole area measured at 90 K (b) Loading plots from the result of an MCR algorithm applied in the SPL measurement of a mc-Si solar cell.

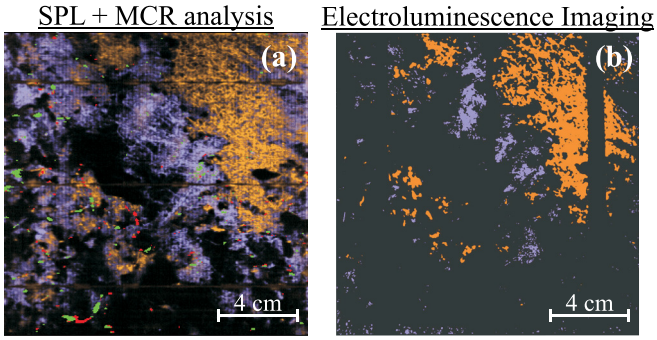

FIG. 3. (a) Lateral distribution of different defect types resolved by MCR algorithm of an SPL measurement (SPL + MCR) on a solar cell. The colours correspond to the defect types distinguished in Fig. 2(b) (Type-A—purple, Type-B—orange, Type-D07—red, Type-VID3—green) (b) Classification by forward and reverse biased electroluminescence introduced in Ref. 13 for comparison on a neighbouring solar cell. Only Type-A and -B defects were distinguished.

III. RESULTS

A. Classification of recombination active defects by MCR analyses of mc-Si solar cells

In Figure 2(a), the spectral response of an mc-Si solar cell integrated over the whole area measured at 90 K by SPL is shown. Below, the indirect band-to-band transition at ~1.1 eV various defect lines can be detected between 0.55 eV and 1 eV. On the SPL measurement (spectral response connected with the positions), an MCR analysis was applied. An MCR analysis resolves mixtures of different signals by determining the number of constituents, their response profiles, and their estimated concentrations without prior information about their nature and composition automatically. The MCR algorithm results in a separation of five different types shown in Fig. 2(b), which are located at different areas with a different spectral response. These loading plots represent the intensity of each signal in the specific area where it is present. Hence, signals only present in some small spots will make little impact on the whole spectrum in Fig. 2(a), since the graph is an integral of all signals from the sample. The algorithm distinguishes: (i) Regions with a strong band-to-band signal at 1.1 eV (band-to-band—black); (ii) regions with two distinct peaks at 0.94 eV and 1.00 eV (Type-A—purple); (iii) regions with a distinct peak at 0.82 eV (and very weak peaks at 0.94 eV and 1.00 eV—Type-B—orange); (iv) few small spots with 0.72 eV peak (Type-D07—red); and (v) small regions showing very intense spectral response at 0.93 eV (Type-VID3—green) with luminescence intensities almost as strong as from areas with band-to-band luminescence.

In Figure 3(a), the lateral distribution of band-to-band (BB, black), Type-A (purple), Type-B (orange), Type-D07 (red), and Type-VID3 (green) is shown. D07 and VID3 defects are detected at defined, localized positions only. The separated regions (signals BB, A, and B) have a small spatial overlap, hence the different types are located at spatially different areas. Figure 3(b) shows the defect classification introduced in Ref. 14 of a neighbouring solar cell (screen printing was rotated by 90°) in order to compare the defect classification with the SPL + MCR analysis. In Ref. 14, the band-to-band luminescence (>1.1 eV), the defect luminescence (0.73–0.85 eV),[24] and the pre-breakdown luminescence of type-2 pre-breakdown sites[4,6] were used to distinguished Type-A (purple) and Type-B (orange) defects. Although the MCR analysis is automatic and based on mathematical algorithms, the classification performed in Ref. 14 and the MCR analysis are nearly identical. Type-A and Type-B defects were identified as the major defect types in both approaches and at very similar wafer positions. In addition to the much higher lateral resolution of SPL, the reproducibility and accuracy are higher due to the usage of the mathematical

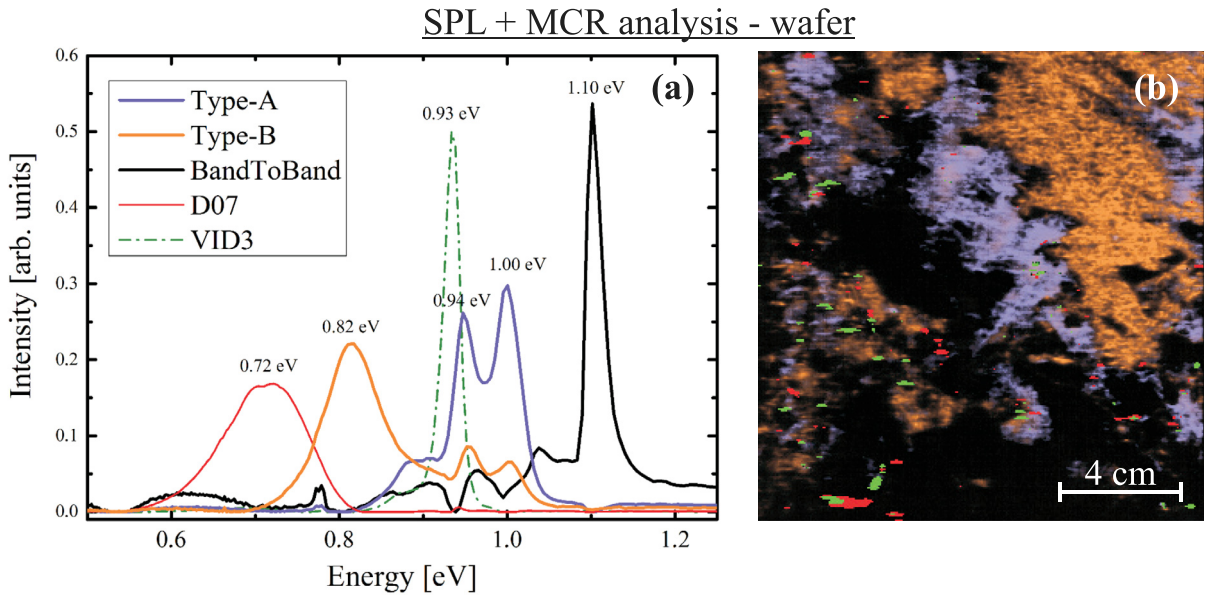

FIG. 4. MCR Analysis of a mc-Si wafer. (a) Spectral response of the defect classes. (b) Lateral position of these defect classes. The same defects were classified on solar cell (Fig. 2) and wafer level. Wafers and solar cells are neighbours.

procedure compared to the manual classification by using electroluminescence methods. Further, it is obvious that using SPL and MCR analyses more Type-A defects are localized. The reason for this will be discussed later.

B. Different defect types on mc-Si wafer level

The same procedure applied in Sec. III A on solar cell level was applied at the wafer level within this section (SPL + MCR) in order to clarify if the specified defect types are already present at wafer level and how they have evolved during the solar cell process. The MCR analysis classifies the same defect types with equal spectral responses as in the case for solar cells as can be seen in Fig. 4.

By comparing the lateral distribution of Type-A and Type-B defects at the wafer (Fig. 4(b)) and the solar cell level (Fig. 3(a)), it can be stated that both defect types are present within equal regions before and after solar cell processing. A closer look reveals that Type-B defects show the same lateral distribution. In contrast, the area covered by Type-A defects are slightly lower compared to the finished solar cell especially close to the left wafer side, which is an edge region near the crucible wall. Note that the lateral distribution of the Type-A and Type-B defects at the wafer level using SPL (Fig. 4(b)) and on solar cell level using luminescence methods (Fig. 3(b)) is rather similar.

C. Spectral response of different types of recombination active defects

The spectral response of the different defect types can be traced back to well-known D-lines. Regions having a low defect density are characterized by a high intensity of the indirect band-to-band luminescence at 1.1 eV with a shoulder below 1.1 eV and missing defect luminescence (cf. Figs. 3(b) and 4(a)). Type-A defects show strong photoluminescence intensities at 0.94 eV and 1.00 eV. These are usually known as D3 and D4 luminescence peaks, respectively.[25] It is often suggested that the D3 line is most probably a phonon-assisted replica of D4.[26] The fact that the MCR algorithm also treats them as one feature (because their spatial distribution is almost identical) can be considered as another hint that both peaks stem from the same defect. Remarkable is a shoulder contributing to Type-A luminescence with low intensity and a peak at around 0.9 eV sometimes observed in microcrystalline thin-film Si layers and attributed to Si-H bonds.[27] This shoulder is responsible for the low defect luminescence intensity (observed by not spectrally resolved PL in the range of 0.73–0.85 eV) at Type-A defects reported in Ref. 14. Type-B defects are characterized by an intense peak at 0.82 eV often denoted as D1 luminescence and not present in regions with type-A defects. Also, here a shoulder can be seen, around 0.88 eV. This might be D2, often mentioned connected to D1.[28,29] Further, additional defect types having defect luminescence at 0.7 eV (Type-D07) and 0.93 eV (Type-VID3) were observed, but these will be discussed in an upcoming publication.

IV. DISCUSSION

A. Lateral distribution of different defect types on solar cell and wafer level

In Section III A it was shown that SPL combined with an MCR algorithm and the defect classification used in Ref. 13 (band-to-band and sub-band EL combined with reverse breakdown behaviour measured by ReBEL) results in the same defect classification of the major defects Type-A and -B. However, Type-D07 and Type-VID3 are additionally classified by the MCR algorithm and were not detected before. The classification is presented using one prominent example, but was proven with different Si materials having different quality. By comparing the EL and SPL classification, it is obvious that the area covered by Type-A defects seems lower using EL methods (cf. Figs. 4(a) and 4(b)). This is likely caused by the methods used. Using EL methods for classification only the pre-breakdown behaviour of type-2[30] under reverse bias (-11 V) is used to locate Type-A defects on solar cell level. At these positions, metal precipitates are present.[31] Under high magnification, these positions are called Type-A_P defects (which corresponds exactly to the positions where metal precipitates is located) in Ref. 14. Type-A_G defects which are the defects in regions close to Type-A_P defects are likely contaminated by atomic impurities since they become activate after a high temperature treatment. Using now the spectral fingerprint of Type-A defects, SPL is the more reliable method for correct localization. Type-B defects show rather the same lateral distribution using SPL or EL methods.

The analysis of the neighbouring wafer in Section III B reveals that all defect types are already present in the wafer material before solar cell processing. Hence, Type-A, Type-B, Type-D07, and Type-VID3 defects are bulk material defects and not induced during solar cell processing. Hence, the root cause for these defects is found in the Si bulk material. Using SPL, the defects can be distinguished already at wafer level. By comparing the SPL measurement before and after the solar cell process a slight activation of Type-A defects can be seen as reported by Bakowskie *et al.*[32] This observation was already discussed in Ref. 14. Likely, metal precipitates are dissolved during the solar cell process from the metal precipitates present in Type-A regions and segregate to grain boundaries during cool down after the p-n junction formation at 850 °C leading to increased recombination activity. All classified defects are found in regions having a high density of crystal defects. In Ref. 14, it is shown that Type-A and Type-B defects can be traced back to grain boundaries or line shaped dislocations. In a future work, this will be investigated by SPL as well.

B. Recombination processes at different defect types

Type-A defects are characterized by D4 (1.00 eV) defect luminescence with the phonon replica D3 (0.94 eV). Beside various discussions about the root cause, D3 and D4 lines are often attributed to stress induced intra-band defect levels energetic very close to the valence and conduction band.[26] However, the energetic position of these defect levels does

not explain the strong recombination activity of Type-A defects reported in Ref. 15 but can explain the luminescence at these defects. In Ref. 14, root cause analyses and the recombination strength as a function of the temperature was investigated. These experimental observations are in good agreement with modelling results of Kveder *et al.*[9] explaining the recombination via a large number of deep defect levels. We assume that at Type-A defects, non-radiative recombination is dominant due to metal impurities. Only a small number of the induced charge carriers recombine via band near defects causing the observed luminescence. The grain boundary character of Type-A defects vary from random angle to even small angle grain boundaries.[33] A possible explanation for the high recombination activity at small angle grain boundaries was given recently by Bauer *et al.*[34,35] who have shown that the increased recombination can be traced back to Lomer dislocation likely contaminated with metals.

Type-B defects are characterized by an intense peak at 0.82 eV denoted as the D1 line. Often D1 is attributed to oxygen impurities.[36,37] However, no direct proof has been found so far. The energetic position of the defect level is in agreement to our previous observations explaining the recombination process via a band near defect level causing defect luminescence and the low influence on the solar cell efficiency. Type-B defects are often traced back to small angle grain boundaries.[33] Therefore, at Type-B defects radiative recombination is dominant rather than non-radiative recombination.

Type-D07 and Type-VID3 will be in focus in an upcoming publication. Krause *et al.*[38] assume that the very intense and local Type-VID3 (near the D3 line) is caused by a specific dislocation network formed at slightly misoriented local Σ3 grain boundary parts.

V. SUMMARY

By applying SPL combined with an MCR algorithm on the spectral photoluminescence response of mc-Si solar cells, the recombination active defects are distinguished without any pre-assumptions made into different defect types: (i) Type-A, (ii) Type-B, (iii) Type-VID3, and (iv) Type-D07. Using SPL, these defects can also be distinguished at the wafer level. Hence, it is concluded that the defects are not introduced by the solar cell process and are already present within the Si bulk material. However, the recombination strength can be changed during solar cell processing. Further, typical spectral responses of the distinguished defects are shown. Type-A defects are characterized by D4 (1.00 eV) defect luminescence with the phonon replica D3 (0.94 eV), Type-B by an intense peak at 0.82 eV denoted as the D1 line, Type-D07 by a peak at about 0.7 eV and Type-VID3 by a very intense peak at 0.93 eV. It is concluded that (i) non-radiative recombination are dominant at Type-A defects and (ii) radiative recombination are dominant at Type-B defects.

[1]J. David Zook, "Effects of grain boundaries in polycrystalline solar cells," Appl. Phys. Lett. **37**(2), 223 (1980).
[2]A. A. Istratov and E. R. Weber, "Electrical properties and recombination activity of copper, nickel and cobalt in silicon," Appl. Phys. A: Mater. Sci. Process. **66**(2), 123–136 (1998).
[3]M. Kittler, W. Seifert, and O. Krüger, "Electrical behaviour of crystal defects in silicon solar cells," Solid State Phenom. **78–79**, 39–48 (2001).
[4]W. Kwapil, P. Gundel, M. C. Schubert, F. D. Heinz, W. Warta, E. R. Weber, A. Goetzberger, and G. Martinez-Criado, "Observation of metal precipitates at prebreakdown sites in multicrystalline silicon solar cells," Appl. Phys. Lett. **95**(23), 232113 (2009).
[5]O. Breitenstein, J. Bauer, K. Bothe, W. Kwapil, D. Lausch, U. Rau, J. Schmidt, M. Schneemann, M. C. Schubert, J.-M. Wagner, and W. Warta, "Understanding junction breakdown in multicrystalline solar cells," J. Appl. Phys. **109**(7), 71101 (2011).
[6]D. Lausch, K. Petter, H. Von Wenckstern, and M. Grundmann, "Correlation of pre-breakdown sites and bulk defects in multicrystalline silicon solar cells," Physica Status Solidi RRL **3**(2–3), 70–72 (2009).
[7]S. Steingrube, O. Breitenstein, K. Ramspeck, S. Glunz, A. Schenk, and P. P. Altermatt, "Explanation of commonly observed shunt currents in c-Si solar cells by means of recombination statistics beyond the Shockley-Read-Hall approximation," J. Appl. Phys. **110**(1), 14515 (2011).
[8]H. C. Card and E. S. Yang, "Electronic processes at grain boundaries in polycrystalline semiconductors under optical illumination," IEEE Trans. Electron Devices **24**(4), 397–402 (1977).
[9]V. Kveder, M. Kittler, and W. Schröter, "Recombination activity of contaminated dislocations in silicon: A model describing electron-beam-induced current contrast behavior," Phys. Rev. B **63**, 115208 (2001).
[10]J. P. Hirth, "The influence of grain boundaries on mechanical properties," Metall. Trans. **3**(12), 3047–3067 (1972).
[11]C. H. Seager, "Grain boundary recombination: Theory and experiment in silicon," J. Appl. Phys. **52**(6), 3960 (1981).
[12]R. Bakowskie, G. Kesser, R. Richter, D. Lausch, A. Eidner, P. Clemens, and K. Petter, "Fast method to determine the structural defect density of 156 × 156 mm^2 Mc-Si wafers," Energy Proc. **27**, 179–184 (2012).
[13]D. Lausch, K. Petter, B. Henke, R. Bakowskie, S. Schweizer, and C. Hagendorf, "Classification of recombination active defect structures in multicrystalline silicon solar cells," Energy Proc. **8**, 28–34 (2011).
[14]D. Lausch, K. Petter, R. Bakowskie, J. Bauer, O. Breitenstein, and C. Hagendorf, "Classification and investigation of recombination-active defect structures in multicrystalline silicon solar cells—recombination models," in *Proceedings of the 27th EUPVSEC*, Frankfurt (Main), Germany (2012), pp. 723–728, see URL https://www.eupvsec-proceedings.com/proceedings/checkout.html?paper=17019.
[15]D. Lausch and C. Hagendorf, "Influence of different types of recombination active defects on the integral electrical properties of multicrystalline silicon solar cells," J. Solar Energy **2015**(4), 1–9.
[16]T. Fuyuki, H. Kondo, T. Yamazaki, Y. Takahashi, and Y. Uraoka, "Photographic surveying of minority carrier diffusion length in polycrystalline silicon solar cells by electroluminescence," Appl. Phys. Lett. **86**(26), 262108 (2005).
[17]T. Trupke, R. A. Bardos, M. C. Schubert, and W. Warta, "Photoluminescence imaging of silicon wafers," Appl. Phys. Lett. **89**(4), 44107 (2006).
[18]E. Olsen and A. S. Flø, "Spectral and spatially resolved imaging of photoluminescence in multicrystalline silicon wafers," Appl. Phys. Lett. **99**(1), 11903 (2011).
[19]A. Flø, I. Burud, K. Kvaal, R. Søndenå, and E. Olsen, "Distribution of radiative crystal imperfections through a silicon ingot," AIP Adv. **3**(11), 112120 (2013).
[20]I. Burud, A. S. Flø, and E. Olsen, "On the origin of inter band gap radiative emission in crystalline silicon," AIP Adv. **2**(4), 42135 (2012).
[21]A. Flø, I. Burud, and E. Olsen, "Spatially and spectrally resolved temperature dependence of defect related luminescence using hyperspectral imaging," in *Proceedings of the Photovoltaic Specialist Conference (PVSC)* (2014), pp. 1888–1892.
[22]J. Bauer, D. Lausch, H. Blumtritt, N. Zakharov, and O. Breitenstein, "Avalanche breakdown in multicrystalline solar cells due to preferred phosphorous diffusion at extended defects," Prog. Photovoltaics Res. Appl. **21**(7), 1444–1453 (2013).
[23]S. Piqueras, L. Duponchel, R. Tauler, and A. de Juan, "Resolution and segmentation of hyperspectral biomedical images by multivariate curve resolution-alternating least squares," Anal. Chim. Acta **705**(1–2), 182–192 (2011).

[24]F. Lausch and C. Hagendorf, "Microscopic Study of Defect Luminescence between 0.72–0.85 eV by optical microscopy," Microsc. Res. **02**(01), 9–12 (2014).
[25]N. A. Drozdov, A. A. Patrin, and V. D. Tkachev, "Recombination radiation on dislocations in silicon," JETP Lett. **23**(11), 597 (1976).
[26]V. V. Kveder, E. A. Steinman, S. A. Shevchenko, and H. G. Grimmeiss, "Dislocation-related electroluminescence at room temperature in plastically deformed silicon," Phys. Rev. B **51**(16), 10520–10526 (1995).
[27]A. U. Savchouk, S. Ostapenko, G. Nowak, J. Lagowski, and L. Jastrzebski, "Band-tail photoluminescence in polycrystalline silicon thin films," Appl. Phys. Lett. **67**(1), 82 (1995).
[28]R. Sauer, J. Weber, J. Stolz, E. R. Weber, K.-H. Küsters, and H. Alexander, "Dislocation-related photoluminescence in silicon," Appl. Phys. A **36**(1), 1–13 (1985).
[29]E. C. Lightowlers and V. Higgs, "Luminescence associated with the presence of dislocations in silicon," Phys. Status Solidi A **138**(2), 665–672 (1993).
[30]J.-M. Wagner, J. Bauer, and O. Breitenstein, "Classification of pre-breakdown phenomena in multicrystalline silicon solar cells, Bd. 24," in *Proceedings of the 24th EU-PVSEC*, Munich, Germany (2009), pp. 925–929.
[31]A. Hähnel, J. Bauer, H. Blumtritt, O. Breitenstein, D. Lausch, and W. Kwapil, "Electron microscope verification of prebreakdown-inducing α-FeSi2 needles in multicrystalline silicon solar cells," J. Appl. Phys. **113**(4), 44505 (2013).
[32]R. Bakowskie, R. Lantzsch, T. Kaden, K. Eller, D. Lausch, Y. Ludwig, and K. Petter, "Comparison of recombination active defects in multicrystalline silicon by means of photoluminescence imaging and reverse biased electroluminescence," in *Proceedings of the 26th European Photovoltaic Solar Energy Conference and Exhibition* (2010), pp. 1839–1842.
[33]D. Lausch, M. Gläser, and C. Hagendorf, "Determination of crystal grain orientations by optical microscopy at textured surfaces," J. Appl. Phys. **114**(19), 194509 (2013).
[34]J. Bauer, A. Hähnel, H. Blumtritt, H. Deniz, A. Zuschlag, and O. Breitenstein, "Do Lomer dislocations spoil high performance of mc-Si solar cells?," Energy Proc. **77**, 565–571 (2015).
[35]J. Bauer, A. Hahnel, P. Werner, N. Zakharov, H. Blumtritt, A. Zuschlag, and O. Breitenstein, "Recombination at Lomer dislocations in multicrystalline silicon for solar cells," IEEE J. Photovoltaics **6**(1), 100–110 (2016).
[36]S. Pizzini, M. Acciarri, E. Leoni, and A. Le Donne, "About the D1 and D2 dislocation luminescence and its correlation with oxygen segregation," Phys. Status Solidi B **222**(11), 141–150 (2000).
[37]K. Bothe, R. J. Falster, and J. D. Murphy, "Room temperature sub-bandgap photoluminescence from silicon containing oxide precipitates," Appl. Phys. Lett. **101**(3), 32107 (2012).
[38]C. Krause, D. Mankovics, H.-M. Krause, T. Arguirov, and M. Kittler, "On the origin of intense luminescence at 0.93 eV from multi-crystalline silicon," J. Appl. Phys. **114**(3), 34902 (2013).